Simultaneous EEG-fMRI: Trial level spatio-temporal fusion for hierarchically reliable information discovery

Li Dong [a], Diankun Gong [a], Pedro A. Valdes-Sosa [a,b], Yang Xia [a], Cheng Luo [a], Peng Xu [a], Dezhong Yao [a,*]

[a] The Key Laboratory for NeuroInformation of Ministry of Education, School of Life Science and Technology, University of Electronic Science and Technology of China, Chengdu 610054, China
[b] Cuban Neuroscience Center, School of Life Science and Technology, Havana, Cuba

ARTICLE INFO

ABSTRACT

Simultaneous electroencephalography (EEG) and functional magnetic resonance imaging (fMRI) have been pursued in an effort to integrate complementary noninvasive information on brain activity. The primary goal involves better information discovery of the event-related neural activations at a spatial region of the BOLD fluctuation with the temporal resolution of the electrical signal. Many techniques and algorithms have been developed to integrate EEGs and fMRIs; however, the relative reliability of the integrated information is unclear. In this work, we propose a hierarchical framework to ensure the relative reliability of the integrated results and attempt to understand brain activation using this hierarchical ideal. First, spatial Independent Component Analysis (ICA) of fMRI and temporal ICA of EEG were performed to extract features at the trial level. Second, the maximal information coefficient (MIC) was adopted to temporally match them across the modalities for both linear and non-linear associations. Third, fMRI-constrained EEG source imaging was utilized to spatially match components across modalities. The simultaneously occurring events in the above two match steps provided EEG-fMRI spatial–temporal reliable integrated information, resulting in the most reliable components with high spatial and temporal resolution information. The other components discovered in the second or third steps provided second-level complementary information for flexible and cautious explanations. This paper contains two simulations and an example of real data, and the results indicate that the framework is a feasible approach to reveal cognitive processing in the human brain.

© 2014 Elsevier Inc. All rights reserved.

Introduction

As noninvasive recording techniques, simultaneous electroencephalography (EEG) and functional magnetic resonance imaging (fMRI) have become widely adopted tools applied in cognitive and clinical neurosciences (Herrmann and Debener, 2008; Huster et al., 2012). Based on measuring changes in the blood oxygen level-dependent (BOLD) signal, fMRI provides high spatial resolution in imaging brain activity but is limited in its low temporal resolution; however, electroencephalography (EEG) has superior temporal resolution but low spatial resolution due to the volume conduction effect. Therefore, in view of their respective strengths and weaknesses being complementary, integrating EEG and fMRI may obtain more comprehensive information regarding brain activity with both high spatial and temporal resolutions. With the development of various fusion techniques, the three most influential approaches for EEG-fMRI integration (He et al., 2011; Huster et al., 2012; Rosa et al., 2010) are the following: (1) fMRI-informed EEG, in which spatial information from the fMRI is utilized to assist the inverse problem of electromagnetic source reconstruction (Dale et al., 2000; Lei et al., 2011b; Ou et al., 2010); (2) EEG-informed fMRI, in which the fMRI benefits from extracted EEG feature in specific frequency (Goldman et al., 2002) or time (Debener et al., 2005; Lei et al., 2010; Luo et al., 2010; Philiastides and Sajda, 2007); and (3) symmetric EEG-fMRI fusion, in which EEG and fMRI data are analyzed jointly through a common generative model (Friston et al., 2003; Valdes-Sosa et al., 2009) or in a common data space (Moosmann et al., 2008).

Regarding the fMRI-informed EEG approach (e.g. the fMRI-constrained source imaging), various methods have been realized to guide EEG source estimation (Babiloni et al., 2005; Dale et al., 2000). The ill-posed problem of EEG source reconstruction is moderated with fMRI spatial constraints; therefore, the underlying neural processes may be better revealed, and the spatial resolution of the EEG is enhanced (Babiloni et al., 2005). Moreover, the Bayesian framework approach may relax the direct correspondence between the two modalities (Henson et al., 2010; Lei et al., 2011b). For EEG-informed fMRI, the BOLD responses are always parameterized using a specific and suitable EEG feature such as event-related potential (ERP) amplitudes (Debener et al., 2005), ERP latencies (Benar et al., 2007), synchronization and phase coherence (Jann et al., 2009), power within specific frequency bands (Scheeringa et al., 2009), or time points of spikes (Luo et al., 2010). Methods employing these strategies are useful in both

---

* Corresponding author. Fax: +86 28 83208238.
E-mail address: dyao@uestc.edu.cn (D. Yao).

task-free (resting state) and task experimental conditions. Furthermore, symmetric EEG-fMRI fusion aims to benefit from both modalities while avoiding the bias of either method. Model-driven fusion such as dynamic causal models (DCM) (Friston et al., 2003; Kiebel et al., 2007) based on a generative model that is neurophysiologically grounded is always confronted with the complexity of the model and tedious calculations. In data-driven fusion, a common data space (Moosmann et al., 2008) or feature space (Eichele et al., 2009) is utilized to jointly assess information gained from both modalities with joint independent component analysis (joint ICA) or parallel independent component analysis (parallel ICA). Another parallel framework involves a contemporary realization of the above fMRI-informed EEG imaging and EEG-informed fMRI for a simultaneous EEG-fMRI dataset (Lei et al., 2010). In brief, the first and second approaches always emphasize either the spatial or temporal aspect of the underlying neural processes with help from the strength of one modality to improve the shortcoming of the other modality, and the third approach underlines the common points without bias of the individual strengths.

The above-mentioned methods are adopted in either temporal or spatial matching. For temporal matching, the vast majority of current methodologies are based upon a linear coupling assumption such as joint ICA or Pearson correlation; however, the nonlinearity in the relationships between the two modalities should be considered (He and Liu, 2008; He et al., 2011). Recently, built on entropy and mutual information of random variables, a novel measure of association called the Maximal Information Coefficient (MIC) was proposed to detect the relationships between variable pairs in large data-sets (Reshef et al., 2011). Due to the generality of this method, a wide range of relationships, whether a linear or a nonlinear relationship and whether with a known or unknown function, should be able to be reasonably captured. By its equitability, it roughly equals the squared correlation (coefficient of determination) of the data relative to the noiseless function. With these well properties, MIC perhaps not only has great potential to reveal the complex relationships between different brain regions in a single modality but also to detect the complex associations between modalities. Regarding spatial matching, the Bayesian framework may be a suitable technique to represent the spatial relationship between EEG and fMRI. Based on this framework, we proposed a method named Network based EEG SOurce Imaging (NESOI) in which multiple fMRI functional networks were used as the covariance priors of the EEG source estimation (Lei et al., 2011b). The hyper-parameters in the model balanced the effects of the fMRI priors and the data fit of the EEG, which determined the contribution of each fMRI prior. More importantly, the EEG and fMRI network information is also matched in the spatial domain with the hyper-parameters (Lei et al., 2011a).

When we analyze these developed methods, we need to emphasize the match integration and also the strengths and shortcomings of each modality. For fMRI-informed EEG source imaging, the intrinsic difference between vascular and electrophysiological responses may result in the fMRI specific source (observed with fMRI but not with EEG) and the EEG specific source (observed with EEG but not with fMRI) (He and Liu, 2008); therefore, the spatial match alone cannot guarantee that the matched events in the EEG inverse are truly the same events in the EEGs and fMRIs. For EEG-informed fMRI, due to the highly different temporal scales and complex relationships between EEG and fMRI, mismatches may also appear in the integration (He et al., 2011). In general, for fusions of EEG-fMRI, two objects should be emphasized: (i) the common substrate of modalities should be identified by the fusion model, and (ii) uncertainty should be decreased when inferring the joint subspace (Daunizeau et al., 2010). Physically, the common substrate of EEG and fMRI should reflect the temporal process of event-related brain activation in the same spatial regions; therefore, a temporal and spatial match is necessary. Certainly, we need to pay attention to the subspaces of EEG or fMRI specificity that may represent the superiority of one measurement and provide the true complementary information of event-related brain activity. Based on these ideas, a hybrid

and hierarchical fusion framework is expected to discriminate among the different situations, the spatio-temporally matched common information space or modality-specific information subspace, ultimately providing hierarchically reliable and meaningful information to explain brain function.

In this work, we propose a hierarchical fusion framework using the recently developed MIC to discover the linear and nonlinear temporal match at the trial level and applying our previous Bayesian approach to realize the spatial match. In addition, a multi-level confidence of the event-related amplitude modulation brain activity is hierarchized from the spatial or temporal match to the spatial–temporal match. Two simulations were implemented in which one simulation involved the potential situations of match or mismatch and the other simulation displayed the linear or nonlinear situation. Finally, an example of real data was illustrated to demonstrate the performance and distinctive features of our hierarchical framework to reveal cognitive processing in the human brain.

Method

Spatio-temporal fusion framework

As the first step of the approach, we subjected EEG and fMRI data to modality-specific preprocessing (more details are observed in real data preprocessing). Temporal ICA (tICA) and spatial ICA (sICA) were performed using EEG and fMRI data, respectively, and subject-specific spatio-temporal information was reconstructed by back-projecting the independent components (Calhoun et al., 2001). The number of independent components was estimated using the minimum description length criteria, which attempts to minimize mutual information between components (Eichele et al., 2011; Li et al., 2007). Second, trial weights onto the fMRI ICA time courses were calculated using the regress model (Eichele et al., 2008), and EEG trial weights were extracted by determining the maximum absolute amplitude. Then, the maximal information coefficient (MIC) between the series of trial weights was calculated to temporally match them across modalities. The hyper-parameter was subsequently obtained to spatially match the components across modalities using NESOI. Finally, hierarchical information of different confidence regarding spatio-temporal fusion was finally obtained. The details of these procedures are summarized in Fig. 1, and the important steps are presented below.

The above steps for simulation were implemented in a customized manner using the code for data generation and visualization. For real data, MATLAB (www.mathworks.com) with the academic freeware toolboxes EEGLAB (http://sccn.ucsd.edu/eeglab), GIFT (http://icatb.sourceforge.org), MINE (http://www.exploredata.net/) and SPM8 (http://www.fil.ion.ucl.ac.uk/spm) was utilized.

Trial weights information

The trial level information was the starting point of the following hierarchical framework. Using temporal and spatial ICA, EEG and fMRI data were decomposed as

$$Y_e = B_e^{n_1 \times p} T_e^{p \times m_1} + \varepsilon_e \tag{1}$$

$$Y_f = B_f^{n_2 \times q} T_f^{q \times m_2} + \varepsilon_f \tag{2}$$

where $Y_e \in R^{n_1 \times m_1}$ is epoched EEG data with n_1 channels and m_1 time points, and $Y_f \in R^{n_2 \times m_2}$ is fMRI data with n_2 voxels and m_2 time points (volumes). B_e are EEG topographies corresponding to p temporal ICA components (T_e), and B_f are the spatial ICA components corresponding to the q fMRI time courses (T_f). ε_e and ε_f are residual errors. In EEG, the amplitudes were obtained as shown in

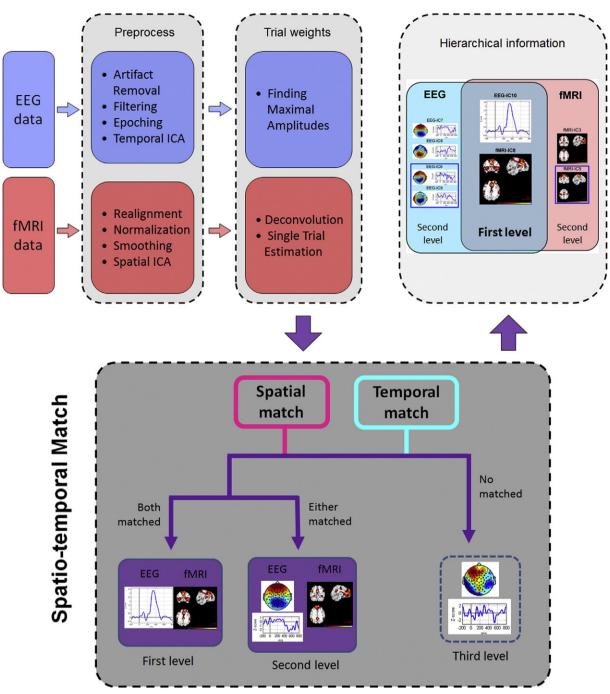$$Z_e = (T_e\{t\})^\top \in R^{k \times p} \tag{3}$$

Fig. 1. The trial level spatio-temporal fusion framework for hierarchically reliable information discovery. Three levels were obtained using spatio-temporal match: first level is associated with the spatio-temporal domain, the second level associated with either the spatial or temporal domains represented a complement information and single modality superiority, and the third level included no matched components and was omitted from this work.

where k is the number of trials, and t is peak time from the absolute maximum of averaged ERPs. In fMRI, two main steps were utilized to obtain the single trial weights of the fMRI data (Eichele et al., 2008). First, the hemodynamic response functions (HRFs) of the fMRI time courses were estimated using the following formula:

$$\widehat{hrf} = M^+ \left(T_f\right)^\top \tag{4}$$

where M^+ is the pseudoinverse of the convolution matrix of the stimulus onsets (assumed kernel length of 24 s) and T_f is the fMRI IC time

course. Then, the fMRI single trial response amplitudes of IC time courses were estimated by the regression model:

$$\left(T_f\right)^\top = (D \otimes hrf)Z_f + \varepsilon \tag{5}$$

$$\widehat{Z_f} = \left(D \otimes \widehat{hrf}\right)^+ \left(T_f\right)^\top \tag{6}$$

where $D \in R^{m_2 \times k}$ is a design matrix containing separate predictors for the onset times of trial, $\otimes$ is the convolution operation, k is the number of

trials, and $Z_f \in R^{k \times q}$ are the amplitudes of fMRI time courses. In these approaches, the amplitude modulations series of EEG (Z_e) and fMRI (Z_f) trial weights were obtained by the trial-by-trial dynamics.

Temporal MIC approach

We used a new exploratory data analysis tool, the maximal information coefficient (MIC) (Reshef et al., 2011), which satisfied the generality and equitability to reveal the temporal relationship of the weight series (Z_e and Z_f) between ICs across modalities. The MIC between the two variables $z_1 \in \{Z_e\}$ and $z_2 \in \{Z_f\}$ is defined as

$$\text{MIC}(z_1; z_2) = \max_{|\mathbb{Z}_1||\mathbb{Z}_2| < G} \left\{ \frac{I^*(\mathbb{Z}_1; \mathbb{Z}_2)}{\log_2\{min\{|\mathbb{Z}_1|, |\mathbb{Z}_2|\}\}} \right\} \quad (7)$$

where $\mathbb{Z}_1$ and $\mathbb{Z}_2$ are the bins of the rectangular grid on the $z_1 - z_2$ scatter plot, and $I^*(.;.)$ is the maximum mutual information achieved by any grid on the data. $|\mathbb{Z}_1||\mathbb{Z}_2| < G$ denotes that the total number of bins is less than some number G. Using real data, the series of trial amplitudes were standardized to z-scores and concatenated across subjects to increase the statistical power before calculating the MIC score. MIC only depends on the rank-order of the data; therefore, the significance of a given MIC score was established by comparing the MIC of the real data with the MIC scores of the surrogate datasets (Steuer et al., 2002). Therefore, by choosing 5000-fold random permutations, null distributions (the variables z_1 and z_2 were statistically independent) for a given sample size were generated, and the p-value of the MIC scores were subsequently obtained. Tests were corrected for multiple comparisons using false discovery rate correction (FDR). In addition, the Pearson correlation coefficient was also calculated, Fisher z-shifted and tested (one sample t-test) as a comparison to assess the performance of the MIC score.

Spatial match

For the i-th topography ($B_e^{(i)} \in R^{n_1 \times 1}, i = 1, ..., p$) of the EEG temporal ICA components, the sources were determined by NESOI (Lei et al., 2011b) using a Parametric Empirical Bayesian (PEB) model (Friston et al., 2006):

$$B_e^{(i)} = L_e \Phi_e^{(i)} + E_{1e} \quad E_{1e} \sim N(0, C_{1e}) \quad (8)$$

$$\Phi_e^{(i)} = 0 + E_{2e} \quad E_{2e} \sim N(0, C_{2e}) \quad (9)$$

where $L_e \in R^{n_1 \times d}$ is the known lead-field matrix calculated for the selected head model, and $\Phi_e^{(i)} \in R^{d \times 1}$ is the unknown distribution of the d dipoles. N(0, C) denotes a multivariate Gaussian distribution with mean 0 and covariance C, and E_{1e} and E_{2e} represent random fluctuations in channel and source spaces, respectively. At the source space level, fMRI ICs (Lei et al., 2011b) and multiple sparse priors (MSPs) (Friston et al., 2008) were included to create covariance priors (C_{2e}) to reconstruct the sources of the topography corresponding to an EEG temporal independent component and was denoted as:

$$C_{2e} = \sum_{i=1}^{q} \gamma_i V\left\{B_f^{(i)}\right\} + \sum_{j=1}^{l} \gamma_j V\left\{MSP^{(j)}\right\} \quad (10)$$

where γ is non-negative hyper-parameter and V is the covariance basis matrix of the spatial ICA components (q components) of the fMRI or MSPs. The hyper-parameters (γ) that controlled the relative contribution of each prior identified whether an EEG component ($B_e^{(i)}$) was able to be considered as an fMRI supported or unsupported component. Model solution can be calculated by the Restricted Maximum Likelihood (ReML) algorithm (Friston et al., 2007), and further details about NESOI can be found in a corresponding paper (Lei et al., 2011b).

Spatio-temporal fusion and hierarchical information discovery

All EEG and fMRI ICs were classified in parallel by temporally matching and spatially matching across modalities. MIC approach was used for temporal matching; and, for spatial matching (using hyperparameters), ERP source analysis was conducted on all EEG components by NESOI, which employed all fMRI components regardless of event-related or event-independent and corresponding MSPs as the covariance priors. Based on the above spatio-temporal matching, three relative reliable information sets were defined as (1) the spatio-temporal matched set that provided the most reliable information regarding common neural processes in both measurements, which was denoted as the first level; (2) either matched set that contained conservative information for one modality, which was denoted as the second level; and (3) the no-matched components set that was not well-explained, which was termed 'noise' and not included in this work. Additionally, to assess the performance of spatio-temporal matching and superiority of the hierarchical framework, the EEG temporal accuracy and fMRI spatial accuracy were evaluated. EEG temporal accuracy was defined as the coefficient of determination (squared correlation) between the time series of the EEG component and the true component. fMRI spatial accuracy was defined as the coefficient of determination (squared correlation) between the spatial distribution of the fMRI component and the true component.

Simulation

Basic setups

To illustrate the previous mentioned framework, a disc with 2452 voxels (dipoles) was employed to generate the simulation data in the trial-by-trial modulation. Areas of 'white matter' were represented by two holes in the disc. For the EEG setup, a concentric three-sphere head model (analytic solution sphere radii: [0.87 0.89 1]) with 128 electrodes placed on the upper hemisphere was set to wrap the disc. The orientations of the EEG sources were fixed, and the lead-field matrix was calculated analytically (Yao et al., 2004). The temporal sampling rate of the EEG was typically 1 kHz, and the epoch of the ERPs was 400 ms, which consisted of 40 time points after being down-sampled to 100 Hz. For the fMRI setup, 2D fMRI spatial maps of 70×70 voxels (one slice) with a field of view (FOV) of 200×200 mm^2 and a Z-axis of 18 mm were hypothesized. In each run, 40 stimuli (trials) were contained in 60 epochs, and a total of 120 stimuli (trials) were presented in 3 runs. Six sources were implemented and drawn with different colors on the disc: 'vision area', 'default mode networks', 'auditory cortex', 'sensory networks', 'left cognition area' and 'right cognition area' (abbreviated as S1–S6). More details regarding the setups were observed in Fig. 2 and Table 1.

Further setups

Through the aforementioned assumed model, two simulations were designed to yield the EEG data and fMRI data. In simulation 1, to consider the different situations of mismatch and match between the vascular and electrophysiological responses, the conventional linear relationships were hypothesized as the trial-by-trial dynamics (represented as amplitude modulation) and further settings were designed below (Fig. 3). For neural sources, S2–S6 were event-related sources, and S1 was a random neuron activity that was simultaneously recorded by EEG and fMRI. For EEG, the S2 signal was blind to detection, and S3 only generated a random electrophysiological activation, meaning that the ERP did not occur. ERPs corresponding to S4–S6 were generated. For fMRI, event-related BOLD responses were generated in S2–S4, and the S5 signal was blind to recording. A random BOLD activation replaced event-related activation as the fMRI signal in S6. In short, for EEG and fMRI, S5 and S2 possessed modality spatial specificity, and S6 and S3 possessed modality temporal specificity.

In simulation 2, with a view to the complex relationship of amplitude modulation in single modality or across modalities, another type
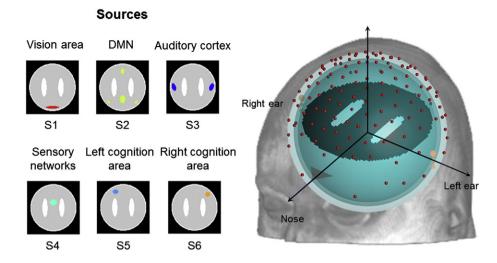
Fig. 2. The primary system of the head model and sources. At left are the source spatial distributions and their names; at right is the simplified concentric three-sphere head model.

of setting was designed to consider nonlinearity. In this situation, S2–S6 were set as event-related sources; however, S1 was a random event-independent, and trial-by-trial dynamic linear or nonlinear functional relationships between the vascular and electrophysiological responses were assumed (Fig. 4). Linear or nonlinear relationships between EEG and fMRI were occasionally assumed for both signals in the same regions or different regions. These functional relationships were linear, quadratic, cosinusoidal and in the form of a parametric equation (Reshef et al., 2011) (Table 2). In view of the occasional signal detection failure, the S2 and S5 signals were blind for EEG and fMRI recording, respectively. In brief, when induced by stimulation, S3–S4 and S6 were spatio-temporal-related sources, and S2 and S5 were modality-specific sources.

Different Gaussian noise with independent and identical distributions (IID) was added to each dataset in both of the above-mentioned two simulations, and a conservative signal-to-noise ratio (SNR) of 0.1 for fMRI and 1.0 for EEG was assumed, and these settings were consistent with typical experimental data. In addition, the whole simulation process was repeated 500 times to obtain mean results.

Real data test

Subjects

After written informed consent, 14 healthy right-handed volunteers with no history of psychiatric or neurological disorders participated in the experiment (7 women, mean age ± SD: 26.0 ± 3.9 years, age range: 21–37 years). The study was also approved by the local ethics committee of the University of Maastricht.

Task

The task comprised four runs of 280 auditory stimuli that consisted of rare sine tones (probability 9%), unique environmental sounds (9%, serving as novel sounds) (Schneider et al., 2008), and frequent standard sine tones (82%, 10 ms rise and fall time, 350 or 650 Hz). Sounds were auto-played through MR-compatible earphones (Siemens Medical Systems, Erlangen, Germany) using Presentation 9.0 (Neurobehavioral Systems, Albany, CA, USA), and the instructions were shown visually via a mirror mounted on the head coil. Stimulus onset asynchrony varied between 1896 ms and 2104 ms after the onset of the MR pulse, and all stimuli lasted 400 ms. Each run lasted 9 min, and the subjects reported the target count during a 1-min break in between runs. Further details regarding the task were observed in a previous article (Strobel et al., 2008).

EEG and fMRI recording

EEG data were recorded using a 64-channel MR compatible EEG system (Brainproducts, Munich, Germany). The EEG cap consisted of 62 scalp electrodes (Ag/AgCl ring electrodes with built-in 5 kΩ resistors) distributed according to the equidistant scalp sites mounted in a cap system (Easycap, Falk Minow Services, Herrsching, Germany) and two additional electrodes, one placed below the left eye to monitor eye blinks and the other attached at the lower back for electrocardiogram (ECG) recording. The data were referenced to the vertex, recorded with a pass-band of 0.016–250 Hz, and resampled at 5000 Hz.

The fMRI data were recorded using a 3-T Siemens Allegra Scanner (Siemens Medical Systems, Erlangen, Germany). Anatomical T1-weighted images were acquired using the magnetization-prepared rapid acquisition gradient echo (MPRAGE). Generating 192 axial slices, the imaging parameters were as follows: TR/TE = 2300 ms/4.57 ms, field of view = 256×256 mm^2, flip angle = 12°, and voxel size = $1 \times 1 \times 1$ mm^3. Functional images were collected using a gradient-echo echo-planar imaging (EPI) sequence, and the imaging parameters were as follows: TR/TE = 2000 ms/30 ms, flip angle = 90°, field of view = 224×224 mm^2, matrix size = 64×64. 24 sagittal slices were acquired (in-plane resolution = 3.5×3.5 mm^2, thickness/interval = 4 mm/1 mm) in an interleaved order, and 285 volumes were obtained during each run.

Table 1
Parameters of simulation setup.

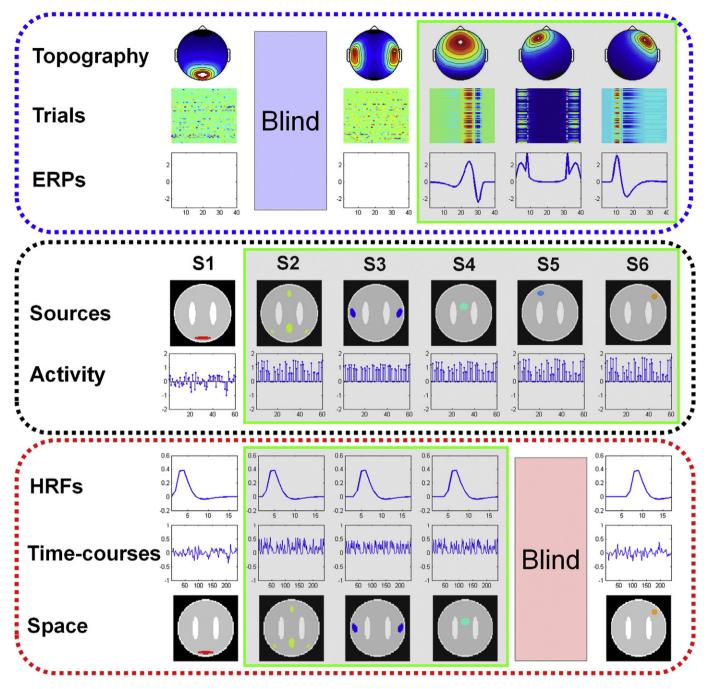|	EEG	fMRI
Sampling frequency	100 Hz	0.5 Hz (TR = 2 s)
Number of time samples	40 points × 60 epochs × 3 runs	240 points × 3 runs
Noise	Gaussian IID	Gaussian IID
Signal-to-noise ratio	1	0.1
Number of channels	128	
HRF		Gamma function with different onset time, and size = 17
Number of stimuli (trials)	120	120
Number of dipoles/voxels per source	S1–S6: [48 100 90 64 32 30]	

Fig. 3. Mismatches and matches between the vascular and electrophysiological responses in simulation 1. Columns from left to right are the names of the features and the source information (S1–S6). For the EEG (upper blue-dashed box), the features include the scalp potential distribution (1st row), single trial images (2nd row) and ERP transient responses (3rd row). For neural activity (middle black-dashed box), the features include the spatial distribution maps (4th row) and the single trial amplitude (5th row). For fMRI (bottom red-dashed box), the features are region-specific HRFs (6th row), time courses of BOLD signals (7th row) and the spatial distribution (8th row). The shaded areas with the green border depict the event-related (also represented as amplitude modulation) sources or recordings.

Real data processing

EEG data were first analyzed using the EEGLAB (http://sccn.ucsd.edu/eeglab), which was run under MATLAB 7. Briefly, gradient artifacts were removed using a local average artifact template procedure (Allen et al., 2000) while a moving average width of 30 MR volumes was used. In addition, the EEG data were 0.3–40 Hz pass-band filtered and down-sampled to 250 Hz. Next, most of the ballistocardiogram artifacts were removed using the OBS-based BCG correction (Niazy et al., 2005), and the residual BCG artifacts were further removed by the ICA

procedure (Srivastava et al., 2005). Using a low pass filter of 15 Hz, epochs from −200 ms to 800 ms were created and re-referenced to the approximate zero reference by free software (Qin et al., 2010; Yao, 2001). To prepare the next calculation, the group tICA was used to decompose the EEG data (64 channels × 24500 points), and the number of independent components was estimated to be 11 using MDL criteria (explaining more than 98% of the variance).

For fMRI data, the first five volumes of each run were first discarded to remove the T1 saturation effects. Next, the standardized preprocess
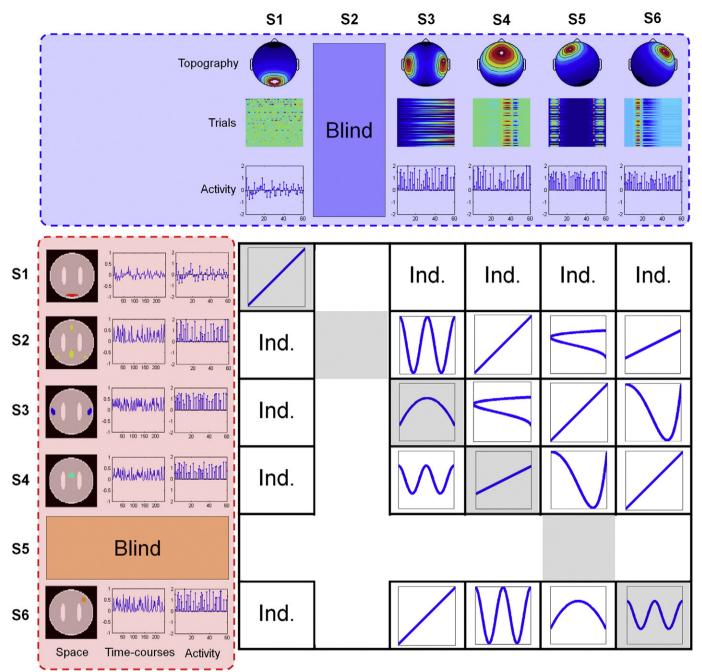
Fig. 4. The linear or nonlinear relationship system in simulation 2. Six different sources (S1–S6) were similarly assumed, and functional relationships of trial-by-trial dynamics (linear or nonlinear) existed (event-related: S2–S6). For EEG (blue-dashed box), the features include the scalp potential distribution (1st row), single trial images (2nd row) and single trial amplitude of caused electrophysiological responses (3rd row). For fMRI (red-dashed box), the features are the spatial distribution (1st column), time-courses of BOLD signals (2nd column) and single trial amplitude of caused BOLD responses (3rd column). The S2 and S5 signals were blind for the EEG and fMRI recording, respectively. The relationships between EEGs and fMRIs in the same region (on the diagonal, shadowed) or different regions (not on the diagonal) are shown in the bottom-right areas to represent the trial-by-trial dynamics. Ind.: Independent.

(slice time correction, 3D motion detection and correction, spatial normalization, and spatial smoothing) was analyzed with SPM8, and the images were sampled to 3 mm × 3 mm × 3 mm and smoothed with a

Table 2
Definitions of the functional relationships.

Relationship name	Description (domain is [0 2])
Linear	$y = x$ or $y = 0.5x$
Parabolic	$y = -(x-1)^2 + 1.5$
Cosinusoidal	$y = c \cdot \cos(2\pi x) + 1$; $c = 1$ or 0.5
Parametric equation	$\begin{cases} y = -(t-1)^2 + 1.5 \\ x = c \cdot \cos(2\pi t) + 1 \end{cases}$; $c = 1$ or 0.5

8-mm full-width at half-maximum of an isotropic Gaussian filter. Using group sICA, the preprocessed fMRI data were decomposed into 14 components (estimated by MDL criterion). Three discarded components visually inspected to be associated with the possible artifacts (such as head motion, cerebrospinal fluid, large vessels and dispersion of clusters) were rejected from further investigation.

After the above-mentioned preprocessing, EEG and fMRI ICs were further analyzed according to the procedure in Fig. 1 to search for the hierarchical reliable information. The amplitude series of EEG and fMRI trial weights (related with target-specific processing) were first obtained, and spatio-temporal match was further investigated using our approach. In addition, EEG-informed fMRI analysis of ERP components

identified in the first level was also conducted to provide possible complementary information for the real data.

Results

Simulation

The mean results were obtained from 500 repeated synthetic datasets, and the results of two simulations are listed below in detail.

Simulation 1: mismatch or match situations

For temporal matching, the temporal integration of the EEG and the fMRI was realized using the MIC approach ($p < 0.05$, FDR corrected), and the results are shown in Fig. 5A. The assumed linear relationships between the sources in the trial were captured by the MIC score. The amplitude modulation components (EEG S4–S6 and fMRI S2–S4) were

successfully extracted and temporally matched between the modalities. Meanwhile, non-temporally matched components (e.g., S1, EEG-S3 and fMRI-S6) were shown on the side. However, the spatial relationships of these temporally matched components were not very clear.

For spatial matching, the EEG ICs and fMRI ICs were spatially matched by NESOI without regard to the temporal relationship between the vascular and electrophysiological responses (Fig. 5B). The truly spatio-temporally consistent component (green bordered area) was contained within the middle matched area, and the spatial specificity of each modality (fMRI-S2 and EEG-S5) is depicted on the sides. However, S3 and S6 (yellow bordered area) were matched; however, the time courses of the EEG and fMRI recordings were mutually independent. In contrast, the S1 (red bordered area) that was not amplitude modulated and recorded by both modalities also appeared in the matched area.

The results of spatial–temporal matching, which is defined as the cross area of the above spatial and temporal matching, are shown in
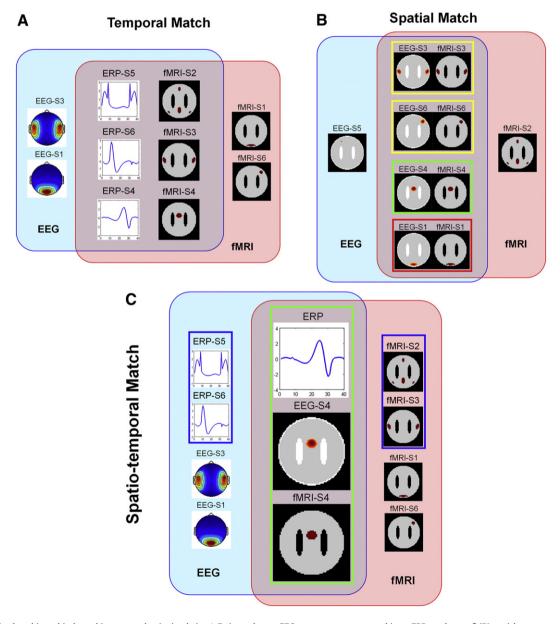

Fig. 5. Results of the three hierarchical matching approaches in simulation 1. Estimated mean EEG sources, mean topographies or ERPs, and mean fMRI spatial components are displayed. A: Temporally matched components are shown in the middle, and non-temporally matched components are shown on each side. B: Spatially matched components are shown in the middle, and the spatial specificities of the single modalities are depicted on each side. C: Hierarchical confidence of the spatial–temporal matching is depicted to reconstruct the brain process. The most credible amplitude modulation components (EEG-S4 and fMRI-S4), which consist of ERP (high temporal resolution), EEG reconstructed source and fMRI spatial distribution (high spatial resolution), are shown in the green bordered region. In the secondary level, temporally matched components are displayed in the blue bordered box, and others are spatially matched components.

Fig. 5C. Linear trial-by-trial dynamics were effectively detected using the MIC approach to extract amplitude modulation components. The spatio-temporal matched components (event-related; EEG-S4 and fMRI-S4) are shown in the green bordered region that contains corresponding ERP (high temporal resolution), EEG reconstructed source and fMRI spatial distribution (high spatial resolution). The specificity of the single modality that temporally (blue bordered area e.g., EEG-S5/S6 and fMRI-S2/S3) or spatially matched (e.g., EEG-S1/S3 and fMRI-S1/S6) was superior (represented as secondary level). Using this method, we obtained hierarchically reliable match results demonstrating that the spatio-temporal matched EEG-fMRI ICs during the trial level were the most reliable and reasonable representations of the underlying brain activity. In addition, the modality-specific ICs that were either matched in the temporal or spatial domain were represented as second-level reliable information that provided complementary information regarding the brain function. No matched components that were observed as the third level were omitted from this work.

In addition, Fig. 6 illustrates that the performance of the spatio-temporal matching and superiority of the hierarchical framework in Fig. 5C was stable and reliable because the standard deviation was very small. The spatio-temporal matched component (event-related, S4) had high EEG temporal accuracy and fMRI spatial accuracy; however, the second levels (concerning event-related fMRI S2/S3 or EEG S5/S6) had single modality accuracy (high temporal or spatial).
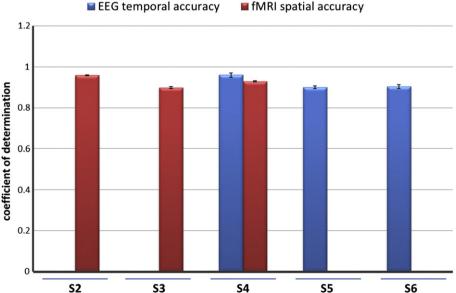
Simulation 2: linear or nonlinear situation

Fig. 7 depicts the results of the linear or nonlinear relationships assumed in simulation 2. Using the one-sample t-test, significant Z-scores of the correlation coefficients were obtained ($p < 0.05$, FDR corrected), and are shown as T-values (see Fig. 7A). For linearity, the correlation coefficient captured the relationship. However, in the case of nonlinearity, the correlation coefficient did not represent the temporal relationship and may capture a plausible relationship if it was independent. For the MIC score, the nonparametric test ($p < 0.05$, FDR corrected) accurately captured the temporal relationship between modalities (Fig. 7B). The MIC score detected the linear or nonlinear relationship but also had ideal ability to distinguish between a relationship and stochastic disturbance. These results clearly demonstrated that the MIC procedure performance was better than the correlation method. Similar to simulation 1, Figs. 7A/B shows the temporal matching, and after similar spatial

matching by NESOI (results omitted here), the final hierarchical spatial–temporal matching result was obtained and is shown in Fig. 7C. The most credible three sources (S3, S4 and S6) are depicted in the green bordered region, and high temporal resolution ERPs are shown to reflect the time process. At the secondary level, temporally matched components (e.g. EEG-S5 and fMRI-S2) are displayed in the blue bordered box, and the other components are spatially matched (S1).

Real data

For the real data, the intermediate results of each modality (such as mean topographies, ERPs, single trial images, and mean fMRI spatial maps) are shown in Figs. S1–S2 in the Supplementary materials. As described in the Method section, hierarchical representation was constructed to discover the brain target processing (Fig. 8). A component of the first level was obtained through temporal ($p < 0.01$) and spatial matching across modalities (Table 3). Corresponding to the EEG-IC10, ERP (absolute amplitude peaking at 336 ms, P300) was shown in the upper middle region, and the regional sources were located in the superior frontal gyrus, superior temporal gyrus, cingulate gyrus, precuneus and inferior frontal gyrus by NESOI. Corresponding to the spatial map of fMRI-IC8, significant regions such as the middle frontal gyrus, cingulate gyrus, superior frontal gyrus, lingual gyrus, middle temporal gyrus and cerebellar tonsil were obtained using one sample t-test ($p < 0.0005$, FDR corrected). The either matched components are shown as the secondary level on each side to explain the target processing. For EEG, the ERPs were peaking at 776 ms, 320 ms, 648 ms, 516 ms, 480 ms and 748 ms in EEG-IC4, IC5, IC6, IC7, IC8 and IC9, respectively (absolute amplitude). For fMRI, spatial distributions located in the insula, parahippocampal gyrus and superior temporal gyrus (fMRI IC2), the anterior part of the default model network (fMRI IC3), the supplementary motor area and postcentral gyrus (fMRI IC5), and the posterior part of the default model network (fMRI IC14) are shown. Further details are shown in Table S1. In addition, the activated regions ($p < 0.01$, FDR corrected) revealed by EEG-informed fMRI analysis mainly consisted of the bilateral superior temporal gyrus (BA22/BA41), culmen, thalamus, medial frontal gyrus (BA6), cingulate gyrus (BA32), precentral gyrus (BA6), inferior frontal gyrus (BA9) and lingual gyrus (BA17/BA18). More details of the results are shown in Fig. S3 and Table S2.

Fig. 6. Mean value and standard deviation of the evaluation metrics (coefficient of determination, R^2) for the hierarchically reliable information in Fig. 5C. Event-related components (S2–S6) are considered.

A **T-values**

	fMRI-S1	fMRI-S2	fMRI-S3	fMRI-S4	fMRI-S6
EEG-S1	5.95		2.29		
EEG-S3			2.70		104.27
EEG-S4		228.31	-67.86	86.80	5.16
EEG-S5		-51.91	173.75	-48.74	-4.92
EEG-S6	2.13	301.04	-70.87	95.99	-4.36

B **MIC scores**

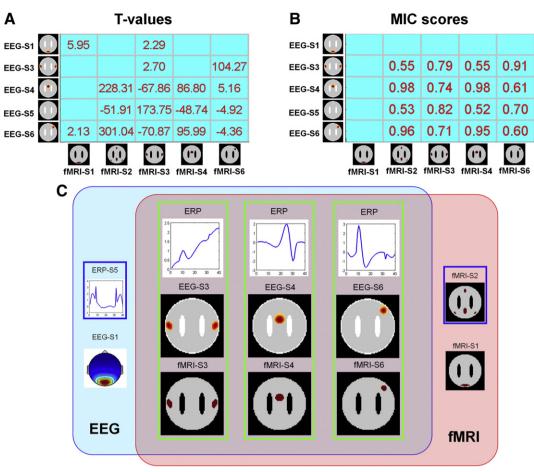|	fMRI-S1	fMRI-S2	fMRI-S3	fMRI-S4	fMRI-S6
EEG-S1					
EEG-S3		0.55	0.79	0.55	0.91
EEG-S4		0.98	0.74	0.98	0.61
EEG-S5		0.53	0.82	0.52	0.70
EEG-S6		0.96	0.71	0.95	0.60

C

Fig. 7. Results of linear or nonlinear situation in simulation 2. Significant T-values of correlation coefficient (A) and MIC scores (B) are shown to reflect the temporal relationships. The significance was set at p < 0.05 and FDR corrected. Corresponding mean fMRI spatial maps and mean EEG sources are also shown. C: Results of the hierarchical spatio-temporal matching are shown with clear hierarchical reliability. The mean event-related EEG sources (in the middle), mean fMRI spatial maps (in the bottom) and corresponding ERP (in the upper) are shown as the first level of the reliability in the green bordered region. In the secondary level, temporally matched components (e.g., ERP-S5 and fMRI-S2) are displayed in the blue bordered box, and others are spatially matched components (S1).

Discussion

Matching and mismatching in integration

In a recent review, the majority of the observed mismatches between EEG and fMRI were interpreted in two ways: (1) a signal detection failure (e.g., activity in deep brain structures cannot be detected by EEG), and (2) a decoupling between the electrophysiological and hemodynamic activity (Rosa et al., 2010). The first aspect was alleviated through spatial NESOI matching (Fig. 5B, EEG S5 and fMRI S2). However, any multimodal EEG/fMRI integration may be confounded by a number of potential decoupling mechanisms. Several sources (Fig. 5B, S3 and S6 in yellow box) may have been spatially matched even though temporal decoupling existed between the EEG and fMRI. In fact, in a specific brain region, fast neuronal oscillations that caused electrophysiological activity and that could be recorded by EEG may not induce any significant BOLD changes (Nunez and Silberstein, 2000), and several ERPs derived from partial phase-resetting of EEG activity may not cause major changes in local brain metabolism to correlate with the BOLD signal (Debener et al., 2006). In contrast, several hemodynamic BOLD changes may be caused by different types of phenomena (e.g., arterial pumping mechanism) that do not correlate with EEGs (Sirotin and Das, 2009). These potential risks should be considered in the integration process to some degree. In addition, several non-neural physiological processes reflected in both modalities (such as muscle contractions that lead to head movement) may be matched using NESOI (Fig. 5B S1 in red box). In the temporal matching approach on the trial level, several temporal decoupling

and non-neural activities were able to be discriminated (Fig. 5A). However, due to the lack of spatial matching information, the matching program may have been confused because the temporal relationships between modalities were widely captured regardless of whether these matched components were co-localized. Potentially, the EEG signal sources generated from the electrical activity of the neuronal population did not necessarily co-localize with the corresponding regions of BOLD signal that was derived from the vascular tree that provided the blood supply to these neurons (Beisteiner et al., 1997). Further analysis and identification should be implemented to reveal more reasonable associations between EEGs and fMRIs.

Hierarchically reliable information discovery

In this work, a spatio-temporal fusion framework was utilized to reconstruct the hierarchical information: the spatial–temporal association between modalities was assumed as the first level in providing reliable information, and the secondary level involved a set of components identified by temporal or spatial matching, which provided complementary information and presented modality superiority (Fig. 5C). The last level included a set of no matched components that were not well explained or were 'noise', and this level was omitted in this work. For the first level, according to its high EEG temporal accuracy and fMRI spatial accuracy (S4 in Figs. 6 and 5C), brain activation was sufficiently explained through this corresponding ERP and fMRI spatial map information as the most reliable information. For components in the secondary level, the temporal information of the EEG (ERPs) components was the
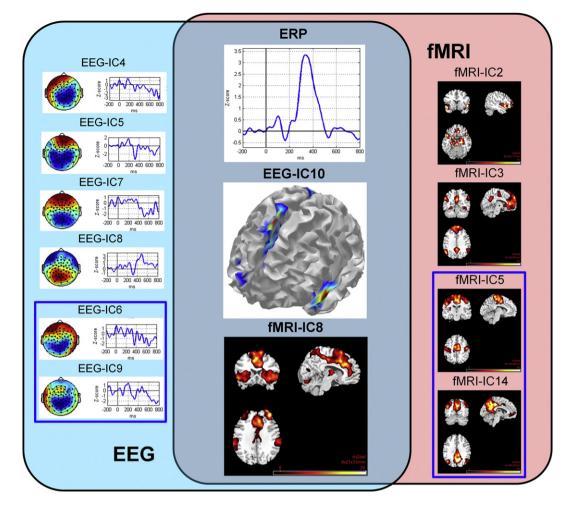
Fig. 8. Results of real data. Hierarchical confidence is depicted to discover the brain target processing. The most credible amplitude modulation components (sources of EEG-IC10 and spatial t-map of fMRI-IC8) and corresponding ERP (Z-score) are shown in the middle region, and the other complementary ERP waveforms (and topographies) or fMRI spatial distributions are displayed as the secondary level on each side. In the secondary level, temporally matched components are displayed in the blue bordered box, and the others are spatially matched components. For the fMRI, the left side of the image corresponds to the left side of the brain.

preferential concerns according to its high temporal resolution. Although EEG sources were reconstructed to some extent using NESOI (Lei et al., 2011b), and considering the potential risk of EEG source imaging such as deep brain structure (Biessmann et al., 2011; He and Liu, 2008; Xu et al., 2007, 2010), the ERPs were previously focused on crude brain regions (temporally matched components S5 and S6 in Figs. 6 and 5C), and the utilization of the source imaging was conservative (i.e., the source imaging of the EEG components was not the first

concern). Regarding the fMRI components in the secondary level, neural activity was measured slowly and indirectly by BOLD response recordings (Buxton et al., 2004); therefore, the spatial distribution (temporally matched components S2 and S3 in Figs. 6 and 5C) was regarded as a certain slow response to neural activity while explaining the type of brain activation. In addition, several components (EEG-S1/S3 and fMRI-S1/S6 in Fig. 5C) that were only spatially matched need to be more conservatively explained. Components in the last level, though omitted from this

Table 3
Spatio-temporal-matched components of the EEGs and fMRIs as first creditability: EEG regional sources and fMRI spatial distributions.

	MNI coordinates			L/R	Sources	Brodmann area		MNI coordinates			L/R	Lobe	Brodmann area	t	Voxels
	x	y	z					x	y	z					
EEG-IC10	8	17	64	R	Superior frontal gyrus	BA 6	fMRI-IC8	36	47	31	R	Middle frontal gyrus	BA 9	23.4	12092
	−55	10	−11	L	Superior temporal gyrus	BA 22		−9	20	37	L	Cingulate gyrus	BA 32	20.8	
	52	14	−14	R	Superior temporal gyrus	BA 38		12	17	61	R	Superior frontal gyrus	BA 6	20.4	
	25	58	12	R	Superior frontal gyrus	BA 10		6	−82	−20	R	Declive	BA18	11.4	668
	−9	17	37	L	Cingulate gyrus	BA 32		−6	−79	4	L	Lingual gyrus	BA 18	10.7	
	6	21	38	R	Cingulate gyrus	BA 32		−6	−73	−5	L	Culmen	BA17/18	8.1	
	3	−54	71	R	Precuneus	BA 7		−57	−58	4	L	Middle temporal gyrus	BA 37	10	70
	44	22	−14	R	Inferior frontal gyrus	BA 47		42	−58	−35	R	Cerebellar tonsil		8.9	107
	−46	21	−5	L	Inferior frontal gyrus	BA 47		33	−58	−35	R	Cerebellar tonsil		7.4	
								−6	−52	−23	L	Fastigium		7.6	39
								3	−58	−38	R	Cerebellar tonsil		6.1	
								−36	−52	−38	L	Cerebellar tonsil		7.3	73
								−30	−61	−32	L	Anterior lobe		7.1	
								−48	−55	−35	L	Cerebellar tonsil		6.8	

work, were not simply useless noise. These components, so called 'noise' that is not directly reflected as amplitude modulation (trial-by-trial dynamics) or are not related to the stimulus, may play a constructive or potential role in neural activity (Ermentrout et al., 2008). Briefly, considering the spatial association and temporal trial-by-trial dynamics, this framework more reasonably identifies the common substrate of EEG and fMRI and decreases the potential uncertainty between these two modalities (Daunizeau et al., 2010).

Linear or nonlinear in integration

In previous studies, an assumption that the neuronal electrophysiological response is linearly correlated with the BOLD fMRI signal has been conventionally shared in various types of fusion techniques, such as EEG-informed fMRI analysis, fMRI-informed EEG analysis or integrating EEG and fMRI; however, to a certain extent, the nonlinearity is acknowledged in the relationships (He and Liu, 2008; He et al., 2011). The source of BOLD nonlinearity has been found in a number of studies, and this nonlinearity may be derived from neural and/or vascular sources (Birn and Bandettini, 2005; Zhang et al., 2008). Moreover, the coupling between neuronal activity and the hemodynamic response may incorporate nonlinear effects and has been discussed in several studies (Liu et al., 2010; Sheth et al., 2004). In addition, the variety of methods to quantify the multimodal signals and the largely different temporal/spatial scales of the hemodynamic and electrophysiological responses may also have partially caused the nonlinearity (He et al., 2011). Considering the potential nonlinearity in trial-by-trial dynamics, using a linear method such as the Pearson linear correlation may lead to false relationships caused by random disturbance and spurious positive or negative linear relationships that were actually nonlinear (Fig. 7A). Hence, a novel measure that has the performance capability to capture a wide range of interesting relationships is expected, especially when we do not know for sure whether the relationship is linear, nonlinear, or even mixed. The MIC score, which possessed good generality and equitability, was utilized to detect the potential relationships between modalities and was demonstrated to capture the assumed functional relationships and suppresses the random disturbance in our simulation (Fig. 7B). Although the nonlinear function relationships we set in the simulation were common and limited, Reshef et al. proved that this measure was appropriate for a wide range of relationship types and showed superiority over other methods (e.g., Spearman correlation coefficient, mutual information) (Reshef et al., 2011). As demonstrated in the results of simulation two (Fig. 7C), this spatio-temporal matching framework based on the MIC approach may be a potential and hopeful technique to reveal complex neurovascular coupling. In the first level of real data, relation between amplitude series of EEG-IC10 and fMRI-IC8 perhaps was nonlinear (Fig. S4), and was further demonstrated that nonlinearity perhaps existed in the physiological signals to be integrated.

Application in real data

In the real data test, hierarchical results using our approach unveiled the spatio-temporal characterization of target processing in the trial-by-trial modulation during an auditory novelty oddball (Fig. 8) and provided both EEG and fMRI evidence that amplitude modulation may widely exists in brain function. Multiple networks involved in the attention process have been proposed in previous studies, such as dorsal networks consisting of the intraparietal and superior frontal regions, the ventral network including the temporoparietal and the inferior frontal cortex (Corbetta and Shulman, 2002), and the frontomedial areas comprised of the anterior cingulate as well as the premotor and supplementary motor regions (Bledowski et al., 2004; Strobel et al., 2008). In the first level, the brain activation response to the target-related task was represented in the fMRI spatial map with high spatial accuracy and ERP with high temporal accuracy. These fMRI patterns were similar to

the aforementioned previous studies and may provide further evidences to uncover the brain function related to top-down-driven target-processing with high spatial resolution. In addition, some regions revealed by EEG-informed fMRI analysis were in accordance with the regions identified by fMRI-IC8 to some extent, such as cingulate gyrus and lingual gyrus etc. Results of activation related to amplitudes of P300 in first level further provided the characterization of target-processing, and these results were complementary to uncover the brain function related to target-processing. Furthermore, the ERP (P300) corresponding to these co-localized networks provided another information of the brain attention process in a high temporal resolution. This information reaches the emphasized high spatial and high temporal resolutions of a cognitive process by EEG-fMRI fusion.

In the secondary level, complementary information was observed as superiority of the single modality. For the EEG, various ERPs with different peaks were identified. These ERPs provided electrophysiological evidences that the attention process may be a dynamic process with synergistic activation of a wide range of neurons in various brain regions and electrophysiologically reflected various subcomponent processes involved in the attention process. Regarding the fMRI, two temporally matched components (fMRI IC5 and IC14) and two spatially matched components (fMRI IC2 and IC3) were found. Sensorimotor regions (fMRI IC5) may be explained in terms of a response preparation process (Bledowski et al., 2004; Linden et al., 1999; Strobel et al., 2008), and fMRI IC14 represented the reallocation of processing resources from areas in which task-induced deactivation (TID) occurred to areas identified in task performance (McKiernan et al., 2003, 2006). These four fMRI components also provided hemodynamic evidences that the attention process may be a synergetic process in various brain regions. In addition, although several components in the last level were neither temporally nor spatially matched in this work, they were not useless noise. In fact, these components can be interpreted in terms of event-related electrophysiological (e.g., EEG IC2, seen in Fig. S1) or hemodynamic responses (e.g., fMRI IC9 located in auditory areas, seen in Fig. S2). The above-mentioned information provided complementary evidence to reveal the characterization of target-processing and to help to elucidate the brain attention process.

In addition, in a real situation, it perhaps is hard to perfectly decompose cognitive processing of rapidly changing synchronization of several parallel but interacting brain circuits (e.g. sensory and selective attention etc.) in ERP and fMRI. In our framework, the temporal ICA was used to decompose parallel ERP components in temporal domain. However, for the fMRI with low temporal resolution, spatial ICA was used to obtain information with spatial independence. The complex interacting brain circuits may be decomposed in spatial domain. And these fMRI spatial components provided priors in parametric empirical Bayesian model for ERP source imaging (NESOI), and did not bring any temporal information. Therefore, our framework could also provide important information furthering our understanding of various cognitive processes. For basic voluntary movements or simple sensory stimulations, brain circuits may be easier to decompose in ERP and fMRI than that in complex cognitive process, and our framework can be similarly applied.

Limitation

Several limitations are involved when using this approach. Although the quality of simultaneous EEG and fMRI recordings has improved, a lower signal-to-noise ratio (SNR) than a separate recording is a potential risk to fusion, and effective data preprocessing techniques (e.g., robust artifact removal technique) are suggested to decrease this risk in our framework. In addition, Kinney and Atwal have argued that "equitability" property of MIC is not proven, and the simulation evidence offered by Reshef et al. may be artifactual (Kinney and Atwal, 2013). It is necessary to pay attention to this problem while using MIC to identify the relationships between variables. However, more evidence and

applications are needed to assess this new measurement, MIC, in the future. Furthermore, due to requiring temporal synchronization between modalities in the trial level, we do not suggest utilizing our approach when obtaining separate recording data. In spite of these limitations, further efforts will be considered in future research.

Conclusion

The novelty of our work is hierarchically reliable information discovery realized by a step-by-step spatio-temporal matching fusion between EEG and fMRI signals. The most reliable level includes the components matched in both the spatial and temporal domains, which provides the long-term desired high spatial and temporal resolution information of a cognitive process. High spatial and temporal resolution information is the focus in EEG-fMRI fusion; therefore, these components determine the explanation with more confidence. Second-level information includes either temporally or spatially matched components. Although these components cannot be explained simultaneously in the spatial and temporal domains, each one may provide distinct information of the cognitive process in either the temporal or spatial aspect. Therefore, they reflect the complementary features of the two modalities and may provide information involving an important cognitive neuroscience problem that needs to be further examined.

In detailed realization, temporal matching is implemented by MIC at the trial level for both linear and non-linear relationships. To our knowledge, this is the first effort in mining the non-linear association between EEGs and fMRIs. The spatial matching is conducted by a method named NESOI, which we developed two years ago. The spatial–temporal matching is the cross integration of the above two matching processes and provides the most reliable information, which was confirmed by the two modalities. Synthetic data studies demonstrated the potential of the approach to reveal the correct spatio-temporal relationships, and the real data results showed that the spatial–temporal matching information was in accordance with the current knowledge of attention processing in the human brain; the second-level modality specific information provides further knowledge for the explanation. We assume that this approach will provide further insights into multimodal integration and will likely provide important information furthering our understanding of various cognitive processes. The proposed hierarchical framework is certainly open for any other temporal or spatial matching approach; therefore, a long-term effort is expected to continue this framework in the future.

Acknowledgments

Appendix A. Supplementary data

Supplementary data to this article can be found online at http://dx.doi.org/10.1016/j.neuroimage.2014.05.029.

References

Allen, P.J., Josephs, O., Turner, R., 2000. A method for removing imaging artifact from continuous EEG recorded during functional MRI. NeuroImage 12, 230–239.
Babiloni, F., Cincotti, F., Babiloni, C., Carducci, F., Mattia, D., Astolfi, L., Basilisco, A., Rossini, P.M., Ding, L., Ni, Y., Cheng, J., Christine, K., Sweeney, J., He, B., 2005. Estimation of the cortical functional connectivity with the multimodal integration of high-resolution EEG and fMRI data by directed transfer function. NeuroImage 24, 118–131.
Beisteiner, R., Erdler, M., Teichtmeister, C., Diemling, M., Moser, E., Edward, V., Deecke, L., 1997. Magnetoencephalography may help to improve functional MRI brain mapping. Eur. J. Neurosci. 9, 1072–1077.
Benar, C.G., Schon, D., Grimault, S., Nazarian, B., Burle, B., Roth, M., Badier, J.M., Marquis, P., Liegeois-Chauvel, C., Anton, J.L., 2007. Single-trial analysis of oddball event-related potentials in simultaneous EEG-fMRI. Hum. Brain Mapp. 28, 602–613.
Biessmann, F., Plis, S., Meinecke, F.C., Eichele, T., Muller, K.R., 2011. Analysis of multimodal neuroimaging data. IEEE Rev. Biomed. Eng. 4, 26–58.
Birn, R.M., Bandettini, P.A., 2005. The effect of stimulus duty cycle and "off" duration on BOLD response linearity. NeuroImage 27, 70–82.
Bledowski, C., Prvulovic, D., Goebel, R., Zanella, F.E., Linden, D.E., 2004. Attentional systems in target and distractor processing: a combined ERP and fMRI study. NeuroImage 22, 530–540.
Buxton, R.B., Uludag, K., Dubowitz, D.J., Liu, T.T., 2004. Modeling the hemodynamic response to brain activation. NeuroImage 23 (Suppl. 1), S220–S233.
Calhoun, V.D., Adali, T., Pearlson, G.D., Pekar, J.J., 2001. A method for making group inferences from functional MRI data using independent component analysis. Hum. Brain Mapp. 14, 140–151.
Corbetta, M., Shulman, G.L., 2002. Control of goal-directed and stimulus-driven attention in the brain. Nat. Rev. Neurosci. 3, 201–215.
Dale, A.M., Liu, A.K., Fischl, B.R., Buckner, R.L., Belliveau, J.W., Lewine, J.D., Halgren, E., 2000. Dynamic statistical parametric mapping: combining fMRI and MEG for high-resolution imaging of cortical activity. Neuron 26, 55–67.
Daunizeau, J., Laufs, H., Friston, K.J., 2010. EEG-fMRI Information Fusion: Biophysics and Data Analysis.
Debener, S., Ullsperger, M., Siegel, M., Fiehler, K., von Cramon, D.Y., Engel, A.K., 2005. Trial-by-trial coupling of concurrent electroencephalogram and functional magnetic resonance imaging identifies the dynamics of performance monitoring. J. Neurosci. 25, 11730–11737.
Debener, S., Ullsperger, M., Siegel, M., Engel, A.K., 2006. Single-trial EEG-fMRI reveals the dynamics of cognitive function. Trends Cogn. Sci. 10, 558–563.
Eichele, T., Debener, S., Calhoun, V.D., Specht, K., Engel, A.K., Hugdahl, K., von Cramon, D.Y., Ullsperger, M., 2008. Prediction of human errors by maladaptive changes in event-related brain networks. Proc. Natl. Acad. Sci. U. S. A. 105, 6173–6178.
Eichele, T., Calhoun, V.D., Debener, S., 2009. Mining EEG-fMRI using independent component analysis. Int. J. Psychophysiol. 73, 53–61.
Eichele, T., Rachakonda, S., Brakedal, B., Eikeland, R., Calhoun, V.D., 2011. EEGIFT: group independent component analysis for event-related EEG data. Comput. Intell. Neurosci. 2011, 129365.
Ermentrout, G.B., Galan, R.F., Urban, N.N., 2008. Reliability, synchrony and noise. Trends Neurosci. 31, 428–434.
Friston, K.J., Harrison, L., Penny, W., 2003. Dynamic causal modelling. NeuroImage 19, 1273–1302.
Friston, K., Henson, R., Phillips, C., Mattout, J., 2006. Bayesian estimation of evoked and induced responses. Hum. Brain Mapp. 27, 722–735.
Friston, K., Mattout, J., Trujillo-Barreto, N., Ashburner, J., Penny, W., 2007. Variational free energy and the Laplace approximation. NeuroImage 34, 220–234.
Friston, K., Harrison, L., Daunizeau, J., Kiebel, S., Phillips, C., Trujillo-Barreto, N., Henson, R., Flandin, G., Mattout, J., 2008. Multiple sparse priors for the M/EEG inverse problem. NeuroImage 39, 1104–1120.
Goldman, R.I., Stern, J.M., Engel Jr., J., Cohen, M.S., 2002. Simultaneous EEG and fMRI of the alpha rhythm. Neuroreport 13, 2487–2492.
He, B., Liu, Z., 2008. Multimodal functional neuroimaging: integrating functional MRI and EEG/MEG. IEEE Rev. Biomed. Eng. 1, 23–40.
He, B., Yang, L., Wilke, C., Yuan, H., 2011. Electrophysiological imaging of brain activity and connectivity-challenges and opportunities. IEEE Trans. Biomed. Eng. 58, 1918–1931.
Henson, R.N., Flandin, G., Friston, K.J., Mattout, J., 2010. A parametric empirical Bayesian framework for fMRI-constrained MEG/EEG source reconstruction. Hum. Brain Mapp. 31, 1512–1531.
Herrmann, C.S., Debener, S., 2008. Simultaneous recording of EEG and BOLD responses: a historical perspective. Int. J. Psychophysiol. 67, 161–168.
Huster, R.J., Debener, S., Eichele, T., Herrmann, C.S., 2012. Methods for simultaneous EEG-fMRI: an introductory review. J. Neurosci. 32, 6053–6060.
Jann, K., Dierks, T., Boesch, C., Kottlow, M., Strik, W., Koenig, T., 2009. BOLD correlates of EEG alpha phase-locking and the fMRI default mode network. NeuroImage 45, 903–916.
Kiebel, S.J., Garrido, M.I., Friston, K.J., 2007. Dynamic causal modelling of evoked responses: the role of intrinsic connections. NeuroImage 36, 332–345.
Kinney, J.B., Atwal, G.S., 2013. Equitability, Mutual Information, and the Maximal Information Coefficient. arXiv, preprint arXiv:1301.7745.
Lei, X., Qiu, C., Xu, P., Yao, D., 2010. A parallel framework for simultaneous EEG/fMRI analysis: methodology and simulation. NeuroImage 52, 1123–1134.
Lei, X., Ostwald, D., Hu, J., Qiu, C., Porcaro, C., Bagshaw, A.P., Yao, D., 2011a. Multimodal functional network connectivity: an EEG-fMRI fusion in network space. PLoS One 6, e24642.
Lei, X., Xu, P., Luo, C., Zhao, J., Zhou, D., Yao, D., 2011b. fMRI functional networks for EEG source imaging. Hum. Brain Mapp. 32, 1141–1160.
Li, Y.O., Adali, T., Calhoun, V.D., 2007. Estimating the number of independent components for functional magnetic resonance imaging data. Hum. Brain Mapp. 28, 1251–1266.
Linden, D.E., Prvulovic, D., Formisano, E., Vollinger, M., Zanella, F.E., Goebel, R., Dierks, T., 1999. The functional neuroanatomy of target detection: an fMRI study of visual and auditory oddball tasks. Cereb. Cortex 9, 815–823.
Liu, Z., Rios, C., Zhang, N., Yang, L., Chen, W., He, B., 2010. Linear and nonlinear relationships between visual stimuli, EEG and BOLD fMRI signals. NeuroImage 50, 1054–1066.
Luo, C., Yao, Z., Li, Q., Lei, X., Zhou, D., Qin, Y., Xia, Y., Lai, Y., Gong, Q., Yao, D., 2010. Imaging foci of epileptic discharges from simultaneous EEG and fMRI using the canonical HRF. Epilepsy Res. 91, 133–142.

McKiernan, K.A., Kaufman, J.N., Kucera-Thompson, J., Binder, J.R., 2003. A parametric manipulation of factors affecting task-induced deactivation in functional neuroimaging. J. Cogn. Neurosci. 15, 394–408.

McKiernan, K.A., D'Angelo, B.R., Kaufman, J.N., Binder, J.R., 2006. Interrupting the "stream of consciousness": an fMRI investigation. NeuroImage 29, 1185–1191.

Moosmann, M., Eichele, T., Nordby, H., Hugdahl, K., Calhoun, V.D., 2008. Joint independent component analysis for simultaneous EEG-fMRI: principle and simulation. Int. J. Psychophysiol. 67, 212–221.

Niazy, R.K., Beckmann, C.F., Iannetti, G.D., Brady, J.M., Smith, S.M., 2005. Removal of FMRI environment artifacts from EEG data using optimal basis sets. NeuroImage 28, 720–737.

Nunez, P.L., Silberstein, R.B., 2000. On the relationship of synaptic activity to macroscopic measurements: does co-registration of EEG with fMRI make sense? Brain Topogr. 13, 79–96.

Ou, W., Nummenmaa, A., Ahveninen, J., Belliveau, J.W., Hamalainen, M.S., Golland, P., 2010. Multimodal functional imaging using fMRI-informed regional EEG/MEG source estimation. NeuroImage 52, 97–108.

Philiastides, M.G., Sajda, P., 2007. EEG-informed fMRI reveals spatiotemporal characteristics of perceptual decision making. J. Neurosci. 27, 13082–13091.

Qin, Y., Xu, P., Yao, D., 2010. A comparative study of different references for EEG default mode network: the use of the infinity reference. Clin. Neurophysiol. 121, 1981–1991.

Reshef, D.N., Reshef, Y.A., Finucane, H.K., Grossman, S.R., McVean, G., Turnbaugh, P.J., Lander, E.S., Mitzenmacher, M., Sabeti, P.C., 2011. Detecting novel associations in large data sets. Science 334, 1518–1524.

Rosa, M.J., Daunizeau, J., Friston, K.J., 2010. EEG-fMRI integration: a critical review of biophysical modeling and data analysis approaches. J. Integr. Neurosci. 9, 453–476.

Scheeringa, R., Petersson, K.M., Oostenveld, R., Norris, D.G., Hagoort, P., Bastiaansen, M.C., 2009. Trial-by-trial coupling between EEG and BOLD identifies networks related to alpha and theta EEG power increases during working memory maintenance. NeuroImage 44, 1224–1238.

Schneider, T.R., Engel, A.K., Debener, S., 2008. Multisensory identification of natural objects in a two-way crossmodal priming paradigm. Exp. Psychol. 55, 121–132.

Sheth, S.A., Nemoto, M., Guiou, M., Walker, M., Pouratian, N., Toga, A.W., 2004. Linear and nonlinear relationships between neuronal activity, oxygen metabolism, and hemodynamic responses. Neuron 42, 347–355.

Sirotin, Y.B., Das, A., 2009. Anticipatory haemodynamic signals in sensory cortex not predicted by local neuronal activity. Nature 457, 475–479.

Srivastava, G., Crottaz-Herbette, S., Lau, K.M., Glover, G.H., Menon, V., 2005. ICA-based procedures for removing ballistocardiogram artifacts from EEG data acquired in the MRI scanner. NeuroImage 24, 50–60.

Steuer, R., Kurths, J., Daub, C.O., Weise, J., Selbig, J., 2002. The mutual information: detecting and evaluating dependencies between variables. Bioinformatics 18 (Suppl. 2), S231–S240.

Strobel, A., Debener, S., Sorger, B., Peters, J.C., Kranczioch, C., Hoechstetter, K., Engel, A.K., Brocke, B., Goebel, R., 2008. Novelty and target processing during an auditory novelty oddball: a simultaneous event-related potential and functional magnetic resonance imaging study. NeuroImage 40, 869–883.

Valdes-Sosa, P.A., Sanchez-Bornot, J.M., Sotero, R.C., Iturria-Medina, Y., Aleman-Gomez, Y., Bosch-Bayard, J., Carbonell, F., Ozaki, T., 2009. Model driven EEG/fMRI fusion of brain oscillations. Hum. Brain Mapp. 30, 2701–2721.

Xu, P., Tian, Y., Chen, H., Yao, D., 2007. Lp norm iterative sparse solution for EEG source Localization. IEEE Trans. Biomed. Eng. 54, 400–409.

Xu, P., Tian, Y., Lei, X., Yao, D., 2010. Neuroelectric source imaging using 3SCO: a space coding algorithm based on particle swarm optimization and l0 norm constraint. NeuroImage 51, 183–205.

Yao, D., 2001. A method to standardize a reference of scalp EEG recordings to a point at infinity. Physiol. Meas. 22, 693–711.

Yao, D., Yin, Z., Tang, X., Arendt-Nielsen, L., Chen, A.C., 2004. High-resolution electroencephalogram (EEG) mapping: scalp charge layer. Phys. Med. Biol. 49, 5073–5086.

Zhang, N., Zhu, X.H., Chen, W., 2008. Investigating the source of BOLD nonlinearity in human visual cortex in response to paired visual stimuli. NeuroImage 43, 204–212.